scientific reports

Check for updates

OPEN

Instrumented swim test for quantifying motor impairment in rodents

Natasha C. Hughes[1], Dale C. Roberts[1], Basile Tarchini[5,6] & Kathleen E. Cullen[1,2,3,4]✉

Swim tests are highly effective for identifying vestibular deficits in rodents by offering significant vestibular motor challenges with reduced proprioceptive input, unlike rotarod and balance beam tests. Traditional swim tests rely on subjective assessments, limiting objective quantification and reproducibility. We present a novel instrumented swim test using a miniature motion sensor with a 3D accelerometer and 3D gyroscope affixed to the rodent's head. This setup robustly quantifies six-dimensional motion—three translational and three rotational axes—during swimming with high temporal resolution. We demonstrate the test's capabilities by comparing head movements of *Gpr156*$^{-/-}$ mutant mice, which have impaired otolith organ development, to their heterozygous littermates. Our results show axis-specific differences in head movement probability distribution functions and dynamics that identify mice with the *Gpr156* mutation. Axis-specific power spectrum analyses reveal selective movement alterations within distinct frequency ranges. Additionally, our spherical visualization and 3D analysis quantifies swimming performance based on head vector distance from upright. We use this analysis to generate a single classifier metric—a weighted average of an animal's head deviation from upright during swimming. This metric effectively distinguishes animals with vestibular dysfunction from those with normal vestibular function. Overall, this instrumented swim test provides quantitative metrics for assessing performance and identifying subtle, axis- and frequency-specific deficits not captured by existing systems. This novel quantitative approach can enhance understanding of rodent sensorimotor function including enabling more selective and reproducible studies of vestibular-motor deficits.

Keywords Phenotypic tests, Balance deficits, Swim test, Head motion, Sensorimotor function, Vestibular, Otolith

Phenotypic characterization of behavioral deficits in mouse and other animal models is an essential aspect of research in the field of neuroscience. Precise and objective characterizations of behavioral deficits enhance the analysis and in turn our understanding of disorders associated with genetic deficiencies or other causes. For disorders caused by impairment of the vestibular system, oculomotor tests, such as measuring the gain and phase of the vestibulo-ocular reflex (VOR) eye movements evoked by head motion, are commonly used (reviewed in[1]). However, while VOR tests provides precise qualitative analysis of vestibular-driven eye movements, they are time-consuming and challenging to perform. Additionally, alone, they fail to capture the specific role of the vestibular system in posture and balance. For instance, mutant animals with impaired peripheral vestibular function may perform normally in VOR tests but exhibit deficits in head movement control, such as tremors[2].

Two common tests for evaluating posture and gait in rodents are the balance beam and rotarod tests, which measure the time taken to cross a narrow beam or fall from a rotating rod[3]. Additional methods, such as videography and footprint analysis, specifically quantify rodent gait[4]. Independently, swim tests have long been valuable indicators of vestibular and sensorimotor defects in rodents[5–8]. This is because during swimming, the water buoyancy attenuates proprioceptive afferent feedback and increases reliance on the vestibular system[9,9]. However, swim test performance is most often not objectively quantified, with deficits frequently described subjectively as 'an inability to swim' or a 'swimming impairment'[11–14]. Moreover, across studies that

[1]Department of Biomedical Engineering, Johns Hopkins University, Baltimore, MD, USA. [2]Department of Otolaryngology-Head and Neck Surgery, Johns Hopkins University School of Medicine, Baltimore, MD, USA. [3]Department of Neuroscience, Johns Hopkins University School of Medicine, Baltimore, MD, USA. [4]Kavli Neuroscience Discovery Institute, Johns Hopkins University, Baltimore, MD, USA. [5]The Jackson Laboratory, Bar Harbor, ME 04609, USA. [6]Tufts University School of Medicine, Boston, MA 02111, USA. ✉email: kathleen.cullen@jhu.edu

use subjective scoring scales of swimming performance, some define '0' as normal while others assign higher score as normal[15,16]. Other studies compare the time an animal spends horizontal, vertical, and sinking[17]. These variations in scoring approaches, combined with the subjective nature of these measures, limit comparisons across studies and laboratories.

Accordingly, we developed the Swimming With Inertial Measurement Unit (SWIMU) test, where a six-dimensional motion sensor is attached to the animal during free swimming. This method allows robust quantitative analysis of three-dimensional translational and rotational motion with high temporal resolution. To demonstrate the test's capabilities, we recorded and compared the head movements of *Gpr156*$^{-/-}$ constitutive mutant mice to their heterozygous littermates[18]. These constitutive mutants lack regional hair cell orientation reversal in otolith organs, resulting in a phenotype not easily detected by most tests, except subjectively scored swim tests[19]. We first present the raw IMU data across all axes, focusing specifically on the linear channels for which the recorded signals comprise two main components: translational head acceleration and head orientation relative to gravity. We then demonstrate the test's ability to selectively detect axis-specific differences in head movements in mutant animals. We also show the test's ability to detect frequency-dependent differences within and across axes. Lastly, we demonstrate the ability to combine the multi-axes data from the SWIMU test into a simple measure of overall performance by analyzing the animal's positional distribution from an upright swimming position. Then, using a probability-weighted average of angular deviation from upright, we are able to accurately separate the mutant mice from the control mice using a simple classifier metric. Together, these findings demonstrate the SWIMU test's robustness and versatility, highlighting its potential as a powerful tool for uncovering vestibular-motor deficits, in various genetic and experimental models.

Results

Comparison of mutant knock-out animals and their heterozygote control littermates: standard testing

For comparison with the instrumented swim test, we first examined constitutive mutant lacking the GPCR GPR156 using standard test. Notably, mutant mice display a specific anatomical deficit, namely a loss of the regional orientation reversal mechanism that normally generates the line of polarity reversal in otolith organs, while hair cell orientation in the semicircular canal cristae remains normal[18]. In line with organ-specific hair cell misorientation, our prior analyses had established that mutant mice display deficits in otolith-driven, but not semicircular canal-driven oculomotor responses that can be quantified via off-vertical-axis rotation (OVAR) versus angular vestibulo-ocular reflex (aVOR) testing, respectively[19]. Additionally, our prior analyses of these mice had revealed no obvious gait or postural deficits,*Gpr156*$^{-/-}$ mutant mice perform normally on balance beam, air righting, contact inhibition and tail hanging tests. Specifically, scored tests such as contact inhibition of righting, air righting, and tail hanging tests all showed no significant differences (Fig. 1A–D, Wilcoxon rank sum test $p = 0.25$, 0.88, $p > 0.999$, $p > 0.999$ respectively, data replotted from[19].

However, while *Gpr156*$^{-/-}$ mutant performance was normal for posture and balance beam testing, when *Gpr156*$^{-/-}$ mice were placed in water, they demonstrated severely impaired swimming compared to controls. Here to independently confirm swimming defects previously revealed by a shorter time to rescue[19], we tested mice during swimming and applied a subjective scoring system (see "Methods"). As shown in Fig. 1E, our subjective analysis of mutant animals' performance in the scored swim test was consistent with balance dysfunction. The most severely affected mutant animals tumbled and rolled, unable to keep their head above water—a marked difference from heterozygote control animals. By scoring animal swimming performance based on the perceived severity of their deficit, significant differences were revealed between the control and mutant animals (Fig. 1E, Wilcoxon rank sum test $p < 0.001$). The potential of the swim test to detect *Gpr156*$^{-/-}$ mutant deficits that cannot be identified by other basic tests reinforces its unique potential to detect balance dysfunction.

Quantative analysis of axis-specific distributions of rotational and linear head motion during swimming reveals defects in *Gpr156*$^{-/-}$ mutant mice

As noted above, although swim tests provide a sensitive assay for identifying balance motor dysfunction, the subjective nature of commonly used scoring measures limits the ability to make robust comparisons between laboratories. Accordingly, we developed an objective test called SWIMU (Swimming with Inertial Measurement Unit) that uses a six-dimensional motion sensor attached to the animal's head during free swimming, enabling the precise analysis of both translational and rotational motion in three dimensions with high temporal resolution. To implement this test, head-posted animals (n = 8 heterozygous, n = 7 homozygous animals) were equipped with a miniature waterproofed SWIMU device consisting of a 3-axis gyroscope and 3-axis accelerometer firmly attached to their head-post. The sensor's wires were kept loose to avoid hindering natural movement. A 40 × 30 × 30 cm tank filled with warm water (24–26 °C) at a depth of 15 cm allowed animals to swim freely[15], and a camera was positioned above for video monitoring and collection. Data was initially collected over a calibration period during which the animals balanced on firm ground (30 s). Following this, animals were placed in the tank where they then swam for up to a minute or until meeting rescue criteria as outlined in the "Methods" section. As shown in Figs. 2 and 3 the head sensor recorded six axes of movement, specifically three axes of linear motion (vertical, foreaft, and lateral acceleration) and three axes of rotational motion (roll, pitch, and yaw rotations), respectively, during each trial. Visual comparison of a 10 s epoch of the time series data recorded from a mutant knock-out animal versus a heterozygote control littermate visually demonstrates the balance deficit in the former. The mutant mice notably exhibited episodes of rapid motion that were particularly evident in the three axes of linear motion (Fig. 2A versus Fig. 3A), reflecting the observed behaviors where mutant animals frequently became unbalanced or flipped. The data from mutant mice is also overall more variable and less consistent, as is visually evident in the higher degree of low-frequency variability of the raw mutant traces

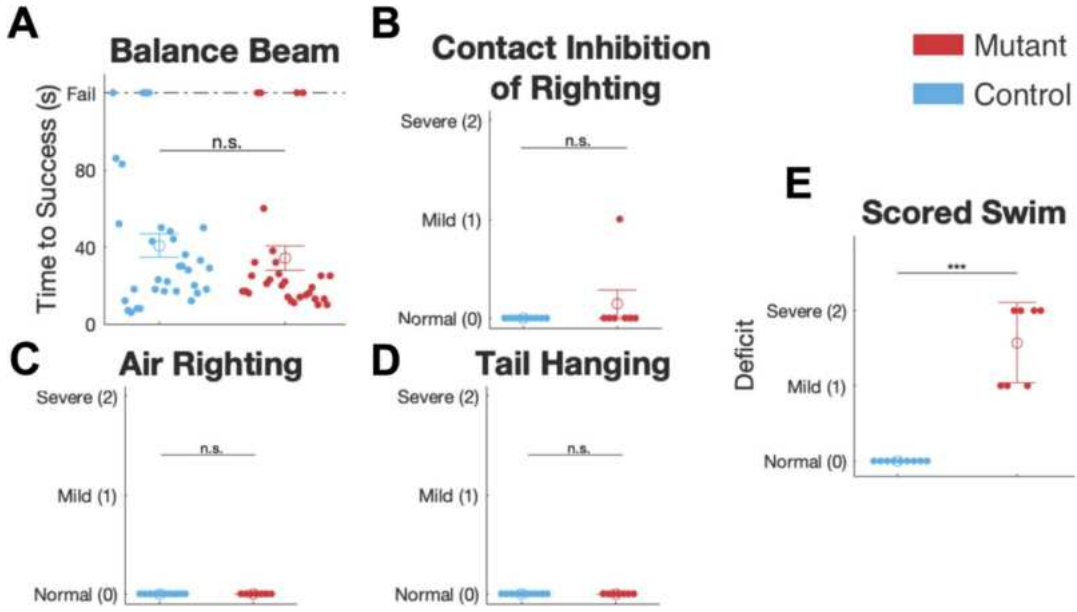

Fig. 1. The swim test gives insight into a dysfunction not observed in other vestibular tests. (**A**) Balance beam time to cross results for a 60 cm long, 6 mm wide beam (Gpr156 + /- n = 10; Gpr156 -/- n = 7). (**B**) Contact inhibition of righting test, in which animal is placed supine with a flat surface laid on top of them in contact with their feet, reveals no significant differences. (Gpr156 + /- n = 9; Gpr156 -/- n = 7) (**C**) Air righting test involves determining severity of deficit based on animal's ability to right their position mid-air, and it reveals no difference between the two animals (Gpr156 + /- n = 10; Gpr156 -/- n = 7). (**D**) Reaching ability of the animal is scored as it is held in air just above a surface in the tail hanging test, revealing no significant differences in the two genotypes. ($Gpr156^{+/-}$ n = 10; $Gpr156^{-/-}$ n = 7). (**E**) In a swim test, subjectively scored performances differ significantly across genotypes ($Gpr156^{-/-}$ n = 9; $Gpr156^{-/-}$ n = 7). (A–D replotted from Ono et al.).

in Fig. 2A, and in broader probability distributions in Fig. 2B. These data demonstrate initial visualization and interpretation of raw IMU data from which we will subsequently derive a concise quantitative metric.

Comparison of the linear head motion generated by mutant versus control animals revealed significant differences along each axis. First, as shown in the population-averaged probability distribution function, we found that the vertical acceleration signal of control animals peaked near 1 g (Fig. 2B). The proximity to 1 g is expected in normal animals, as a component of gravity will act parallel to the animal vertical axis as the animal swims with its head up. In contrast, although the vertical acceleration signal of mutant animals also peaked near 1 g, the kurtosis of the distribution was significantly lower in the mutant population ($p < 0.05$) with greater distribution of vertical acceleration in values lower than 1 g as shown in the probability distribution function, indicating that mutant animals spent less time with gravity parallel to the animal vertical axis (Fig. 2B).

A comparable analysis of the population-averaged probability distribution functions of foreaft acceleration also revealed differences. The peak of this distribution was greater than zero in normal animals, reflecting the animal's forward motion during swim (Fig. 2B). In the mutant animals, however, the probability distribution function was characterized by many values < 0 g and had a much flatter peak. As a result, there were significant differences from control in both the skewness ($p < 0.001$) and kurtosis ($p < 0.01$) of the foreaft distribution. Finally, the lateral probability distribution function is consistent with the instability observed in the mutant animals, although differences in either kurtosis or skew of the lateral acceleration signal of the two groups did not reach significance ($p > 0.05$ for both; Fig. 2B).

Overall, the observed differences in the linear head motion of mutant animals in both the vertical and foreaft axes are consistent with their inability to remain upright during swimming. An equivalent examination of the population-averaged probability distribution functions of rotational motion also revealed significant differences in skewness of roll angular velocity ($p < 0.05$) and in pitch angular velocity kurtosis (Fig. 3B, $p < 0.05$). No notable differences were observed in yaw angular velocity (Fig. 3B). Thus, the observed differences in angular velocity about the pitch and roll axes serve to further quantify the imbalance in the mutant animals' swimming behavior.

In summary, these findings collectively suggest that the instrumented swim test is sensitive to variations across various axes of head motion, allowing for the quantification of differences in mutant animals' swimming behavior. These encouraging results also demonstrate differences in the raw IMU data generated by this method of behavioral quantification and, furthermore, how to interpret these results, which can be initially unintuitive to those unfamiliar with IMU analysis. This lays the groundwork for a more sophisticated frequency-based analysis and examination of three-dimensional orientation, which will be explored below.

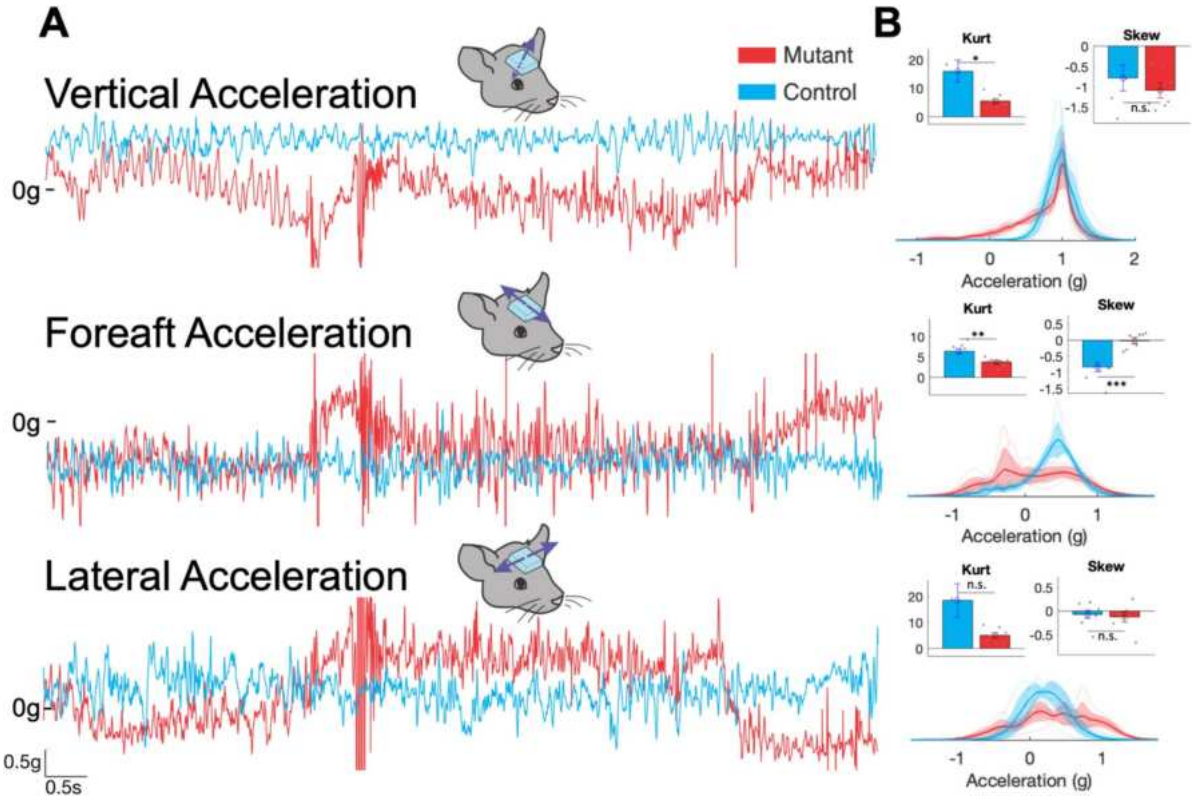

Fig. 2. Raw traces from a head-mounted sensor in two swimming mice and population averaged distributions for each linear head motion axis. (**A**) 10 s sample trace of the vertical acceleration (first row), foreaft acceleration (second row), and lateral acceleration (third row) from accelerometer data (please note that acceleration due to gravity is included in this data) in units of g from a control and from a mutant animal, offset from one another for visual comparison during swim. Scale is at bottom-left. (**B**) Population-averaged probability distribution functions for these signals with corresponding standard deviations shaded. Inset left: Population-averaged kurtosis (left) and skew (right).

Quantative analysis of axis-specific spectral power during swimming reveals defects in *Gpr156*$^{-/-}$ mutant mice

The analysis of the power spectra of head movement across axes has been shown to identify head movement differences in patients with vestibular peripheral loss whereas distributions of linear accelerations and rotational velocities did not[20]. Accordingly, we hypothesized that we would see clear differences in the head movement power spectra of mutant versus control mice during swimming using this same approach. To test this proposal, we computed the power spectra of the head signals generated in each of the six dimensions of motion, as a function of temporal frequency. Quantification of our results are shown in the log–log plots of Fig. 4.

Overall, the six-dimensional motion statistics experienced by normal mice during swimming revealed results similar to those observed during locomotion[21]. Specifically, spectral content motion in each axis showed significant power up to 20 Hz. Furthermore, consistent with our prediction, head movement power spectra were significantly altered in mutant mice. First, we found that mutant mice generated a significant increase in power in all three linear axes (i.e., foreaft, lateral, and vertical) across the frequency range of 0–5 Hz (Fig. 4A–C), such that their mean power across this same frequency range was significantly greater compared to controls (permutation test $p < 0.0001$ in each axis, Fig. 4A–C inset left). Second and correspondingly, we found that mutant mice generated a significant increase in power in all three rotational axes (i.e., roll, pitch, and yaw) across the frequency range of 0–5 Hz (Fig. 4D–F), such that their mean power was also significantly greater than that of controls (permutation test $p < 0.0001$ in each axis, Fig. 4D,E,F left inset figures). Additionally, mutant mice generated greater higher-frequency head motion power (5 to 20 Hz) in the fore-aft and lateral linear axes as well as pitch and yaw rotational axes compared to the controls during swimming (Figs. 4A,B,E,F right inset). Taken together, these results demonstrate that the SWIMU instrumented swim test can detect frequency-dependent differences in head motion, marking a significant advancement. Power spectra analysis enables a comprehensive comparison of all mutant and control trials, providing axis-specific characterization of animal movement across various frequencies that can potentially significantly enhance the detection of behavioral deficits.

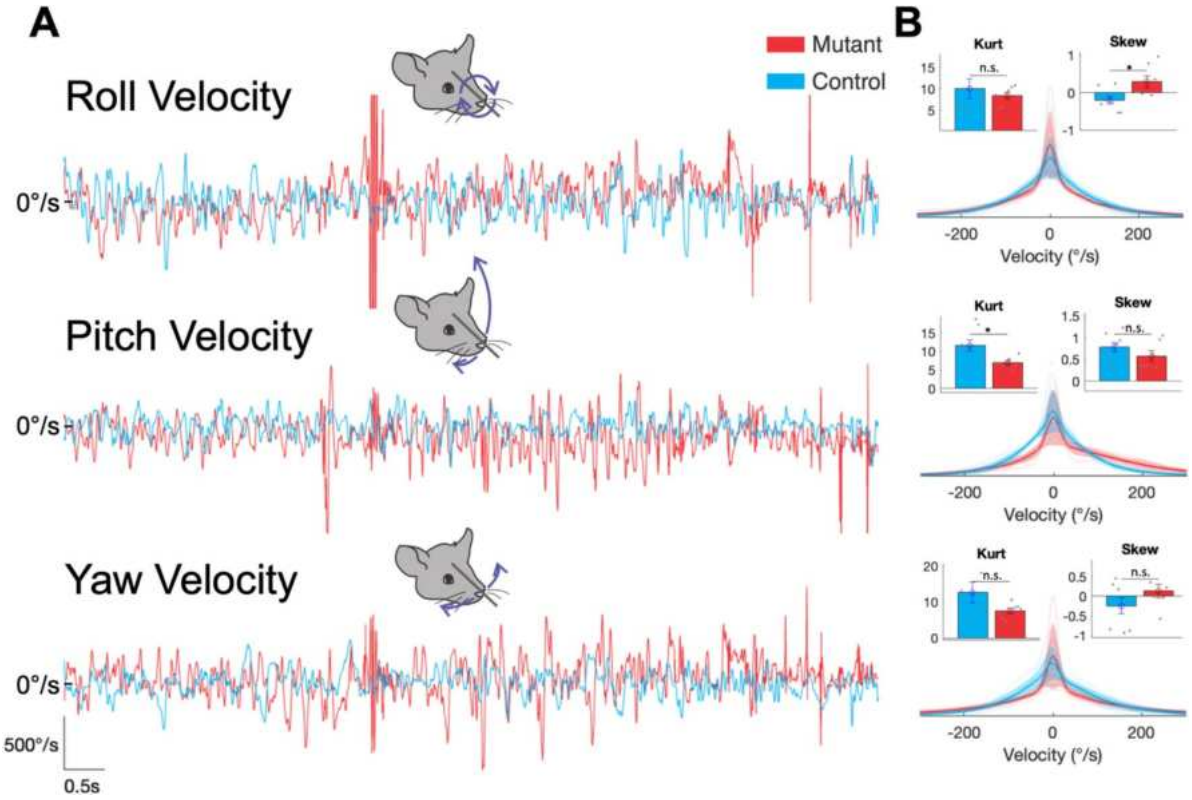

Fig. 3. Raw traces from a head-mounted sensor in two swimming mice and population averaged distributions for each rotational head motion axis. (**A**) 10 s sample trace from the same 10 s as in Fig. 2, showing sample traces of the rotational velocities measuring the velocity in m/s in the axes of roll, pitch, and yaw for both the control and mutant animals, offset from one another for visual comparison. Scale is at bottom-left. (**B**) Population-averaged probability distribution functions for these signals with corresponding standard deviations shaded. Inset: population-averaged kurtosis (left) and skew (right).

SWIMU based spherical representations of animal head orientation in individual trials as a measure of performance

Notably, the axis-specific power spectrum analysis described above considers each axis independently, a common approach in other studies[21]. However, this method alone is not fully comprehensive, as mice simultaneously move in multiple directions across these axes over time. Thus, to complement our axis-specific power spectrum analysis, we next developed a method to graph the orientation of the animal's head to analyze overall performance across all axes, and more easily visualize the ability of each animal to keep its head above water while swimming. To do so, we used MATLAB (MathWorks, Natick, MA) **imufilter()** sensor fusion function, which takes the accelerometer and gyroscope (angular velocity) signals and computes a three-dimensional "heading" orientation coordinate axis (i.e., "mouse head relative to space" coordinates) for each IMU data sample (see detailed explanation in "Methods" section). The axis is zeroed while the mouse is standing, out of water, and we assign the three orthogonal X, Y, and Z coordinate vectors to forward "nose", leftward "ear", and upward (aligned with gravity) "head" (Fig. 5A, left).

We then projected just the animal's upward "head" vector trace over time onto a unit sphere to illustrate the animal's time varying head orientation during each swim trial (Fig. 5A, right). After entering the water, the animal must point its nose upward to keep it out of the water while swimming. Consequently, the head upward vector is no longer aligned with gravity, and as the mouse swims around the tank with its nose pointed upward, the resulting sphere plot shows a circular ring around the "north pole" of the sphere. This is shown in the "top down" view in Fig. 5A, the middle of the three sphere plots. We found the mean of the swimming head pitch to be approximately 45° pitch upwards compared to the out of water head pitch. Accordingly, we used this information to rotate the heading axis data 45 degrees downward, so that the sphere plots would show data close to the "north pole" position during swimming. We thus defined this new "forehead" vector as a vector parallel and opposite to gravity when the animal is swimming in a 45° nose-upwards-pitched position (Fig. 5B,C left).

Using this new forehead vector, we replotted the same control animal trial, which produced a tight circle surrounding the top of the sphere (Fig. 5B). For all control animal trials, the trace of the forehead vector consistently stayed very close to this upright position, reflecting good swimming ability with the head above water. In contrast, the forehead vector trace of *Gpr156*$^{-/-}$ mutant animals did not form a tight circle around upright. Instead, traces encompassed a far larger portion of the sphere as the animal deviated from upright and even flipped upside down (Fig. 5C). To aid in quickly identifying large deviations from upright, the sphere plots

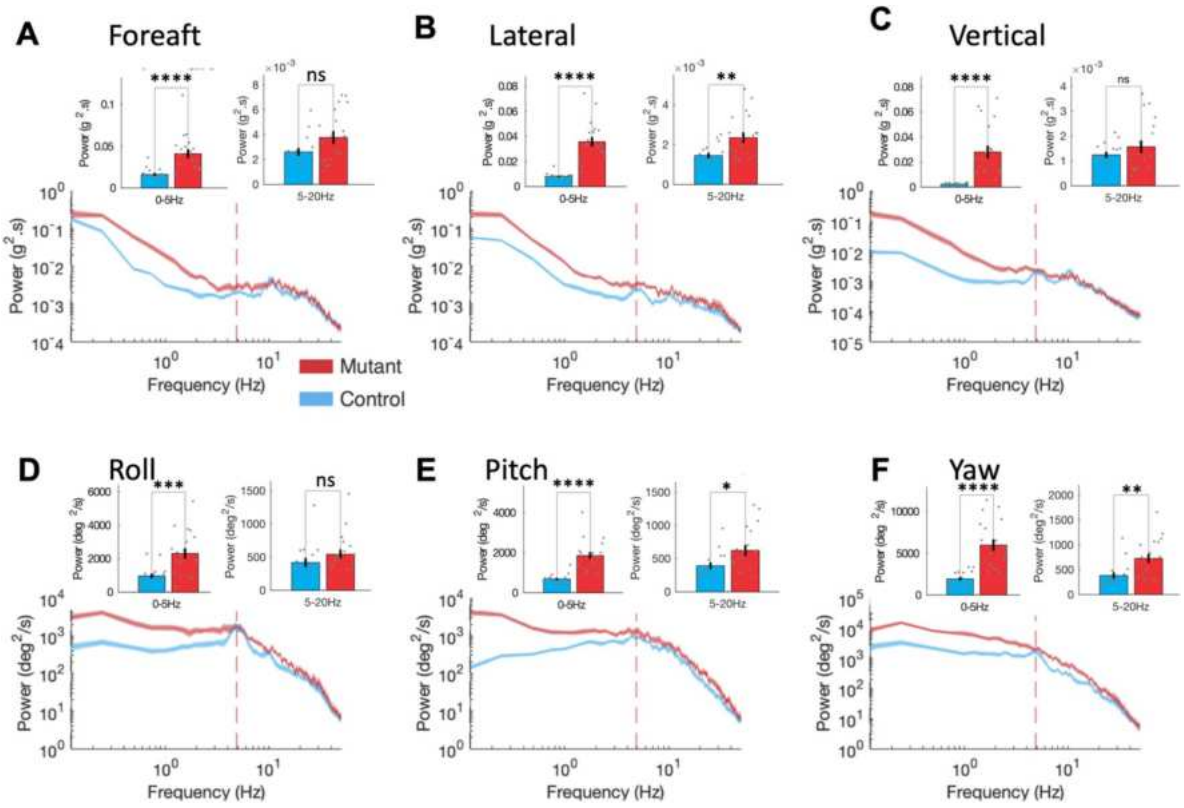

Fig. 4. Characterization of axis-specific power differences in head movement during swim. Red dashed line is at 5 Hz. Inset: Left of red dash is power spectra bars for 0–5 Hz and right of red dash is power spectra bars for 5–20 Hz. Gray dots represent averages from individual trials. (**A**) Foreaft accelerometer power spectra and bars ($p < 0.0001$ for left inset, $p < 0.05$ for right inset). (**B**) Lateral accelerometer power spectra and bars ($p < 0.0001$ for left inset, $p < 0.01$ for right inset). (**C**) Vertical accelerometer power spectra and bars ($p < 0.0001$ for left inset, $p > 0.05$ n.s. for right inset). (**D**) Roll gyroscope power spectra and bars ($p < 0.001$ for left inset, $p > 0.05$ n.s. for right inset). (**E**) Pitch gyroscope power spectra and bars ($p < 0.0001$ for left inset, $p < 0.05$ for right inset). (**F**) Yaw gyroscope power spectra and bars ($p < 0.0001$ for left inset, $p < 0.01$ for right inset).

are colorized orange when the forehead vector deviates between 66 and 90 degrees from upright, and colored red when it deviates more than 90 degrees (indicating that the top of the head is pointing downward, and the animal is essentially upside-down). The spherical plot of animal head deviation from upright provides a clear, simple method for quickly visualizing differences in swimming ability between subjects.

Statistical presentations of the forehead vector deviations-from-upright data

Here we present statistical analyses of the forehead vectors' deviation-from-upright, comparing control to mutant animals. The deviations are taken to be simply the angles that the forehead vector makes with the upright gravity vector as the mouse is swimming. Figure 6A shows the population-averaged deviation-from-upright probability distribution for control (dark blue trace) and mutant (dark red trace) mice. The same plot also shows individual trials as lighter traces, and standard deviation as shading around the dark averaged trace. Note that despite inter-animal variability, the peaks of the individual control mice traces are generally closer to upright compared to the more inconsistent, spread-out probability traces of the mutant mice. The population-averaged skew, kurtosis, and median can also be statistically compared, revealing a significant difference in the median distance from upright (mean median and standard deviation is 46.2° + /- 10.3° for mutant, 18.7° + /- 2.9° for control, $p < 0.001$, Fig. 6B), but not in their skew or kurtoses values ($p > 0.05$ for both).

The results can also be visualized as histograms of head deviations of mutant vs. control mice (Fig. 6C), with the benefit of producing a direct visualization of the raw, binned data as opposed to an average of probability function traces. The histograms align well with the mean probability distribution function when visually compared (Fig. 6A,C). The lower panel in Fig. 6C shows the clear separation between the mutant median distance of 42.7°, and the control's 18.1°. This method demonstrates numerically the mutant's variability in their distance from upright with an interquartile range of 30.4° compared to 14.9° for the controls (Fig. 6C). These two simple analyses of the deviation-from-upright data provide a quantitative comparison of performance across different genotypes using head linear acceleration and angular rate sensor data.

Finally, to demonstrate sensitivity and specificity of our test, we derived a numerical classifier using the probability distribution function data to differentiate mutants from control animals. Specfically, we computed the weighted average of the probability distribution for a given animal, plotted for ease of visualization (Fig. 6A,

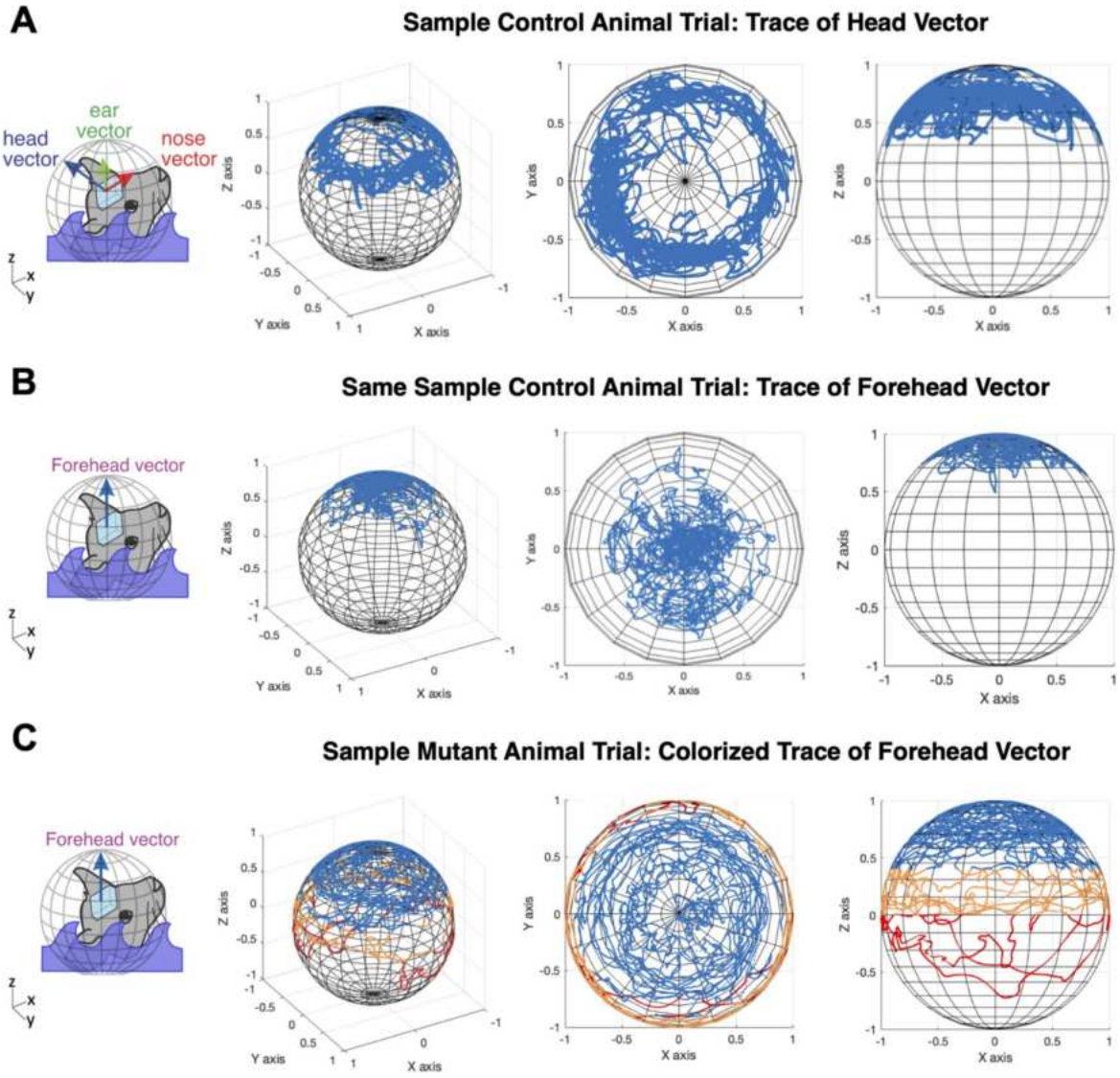

Fig. 5. Spherical representation of animal head orientation to visualize swimming performance. (**A**) Left cartoon shows the three coordinate axis vectors (nose forward, ear leftward, and head upward) representing animal head orientation. Right are three sphere plot views of the same data, showing just the head upward unit vector (ear and nose vectors are not used) from a single control animal trial, traced over time onto a unit sphere. (**B**) Left cartoon shows new forehead vector (blue) which is pitched upward 45 degrees to be nominally aligned with gravity during swimming. Right are three views of the same data from panel A, but now using the forehead vector's trace rather than the head vector, showing tighter alignment to the sphere "north pole". (**C**) Forehead vector plot of a mutant animal, showing considerable deviation from upright. *Only the forehead vector is plotted*, but data are colorized to indicate when the vector is significantly deviated from upright: the trace is orange where the animal forehead vector deviates from upright by 66°-90°, and red when deviation is more than 90°.

inset). With a threshold of 30°, where less than 30° is labelled as a control animal and greater than 30° is labelled as a mutant animal, this metric has 100% true positive rate and 100% true negative rate for this sample and separates the two mouse populations without error (Fig. 6A, inset).

Discussion

In this study we present a novel instrumented swim test that provides a sensitive and objective method for assessing motor performance to identify sensorimotor, most notably vestibular motor, deficits. By measuring head movement differences across six axes of rotational and translational motion we can detect impairments in mutant versus control mice through comparison of the probability distribution for each axis. Additionally, the analysis of power spectra provides the ability to determine whether movements are selectively altered within specific frequency ranges, within and across axes. Further, using an approach based on spherical coordinate we were able to combine the multi-axis data from the SWIMU test into a simple measure of overall performance

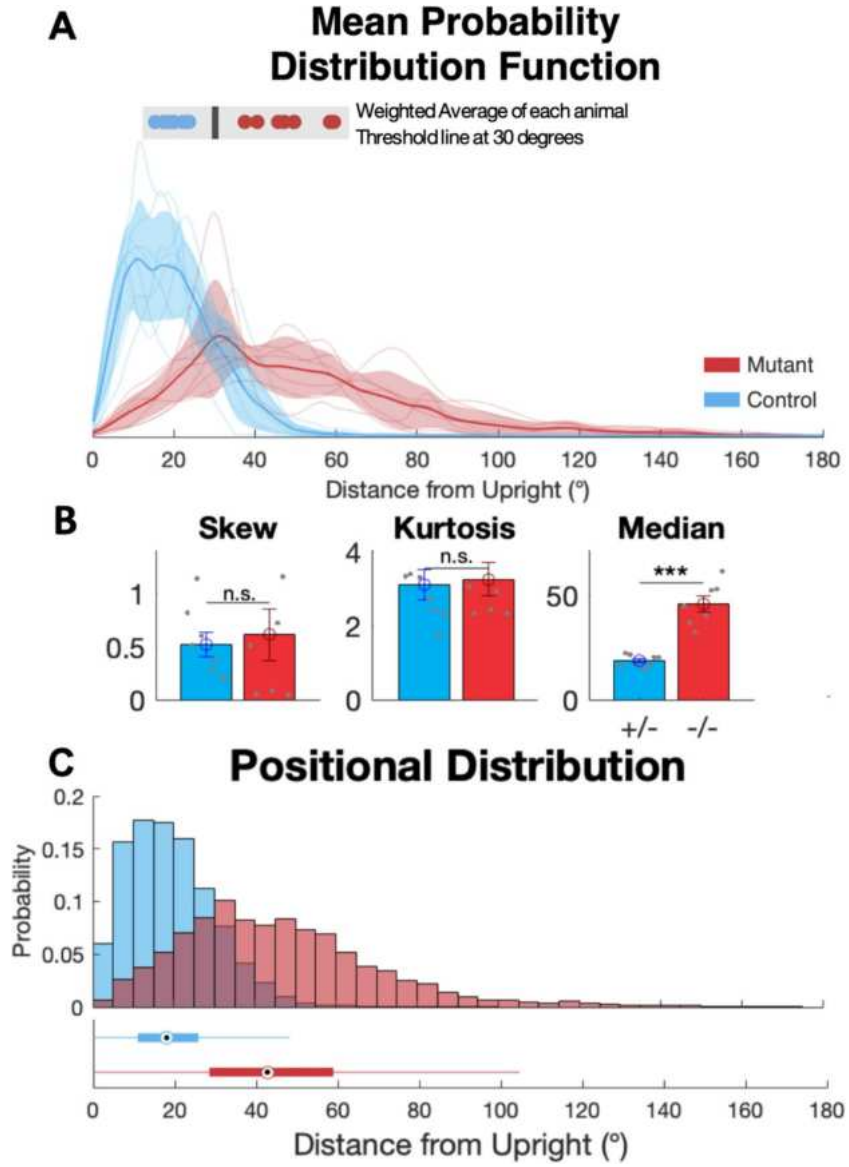

Fig. 6. Statistical presentations of head deviation-from-upright data. (**A**) Population-averaged probability distribution functions of control (BLUE) and mutant (RED) animal forehead vector deviation from upright, with corresponding standard deviations shaded. Individual animals are shown as light traces. Gray shaded inset: Shown is the classifier metric of the weighted average of each animal's forehead vector tracings, with a vertical line representing a threshold of 30° that can be used to differentiate the mutant (red) and control (blue) animals. This inset shares the X axis with the probability traces. (**B**) Population-averaged skew ($p > 0.05$), kurtoses ($p > 0.05$), and median (in degrees, $p < 0.001$) values respectively compared across control and mutant animals. Individual animal data points are shown in gray. (**C**) Histogram with bin size of 5°, including all data from 16 trials for 8 control animals and 20 trials for 7 mutant animals. (**D**) The box plot showing the median (black dot), interquartile range (filled rectangle), and the whiskers corresponding to approximately + /- 2.7 standard deviations for the combined positional distributions shown above in (**C**).

that robustly and objectively quantifies animal's positional distribution from an upright swimming position. From this we demonstrated a simple numerical classifier that identifies our mutant and control animals with 100% accuracy. Overall, our instrumented test allows for precise and reliable quantification of sensorimotor performance, highlighting the instrumented swim test's utility in revealing and identifying vestibular motor deficits.

Implications for testing behavioral deficits in mutant mice

Swimming is a natural and easily testable activity for mice, widely used to evaluate mouse behavior and physiology. It is utilized in psychiatric studies on depression and anxiety via the forced swim test[22] and in studies of vestibular dysfunction as in this paper. Its utility regarding the latter is supported by numerous

studies showing that swimming deficits often result from vestibular deficits[5–8,11,23–26]. Swim tests are particularly sensitive for detecting vestibular deficits compared to other tests like the rotarod and balance beam tests because the buoyancy of the animal in water reduces the load on its limbs, which in turn decreases proprioceptive feedback[10,9]. We found that the SWIMU test was sensitive and specific, able to identify the mutant mouse genotype with 100% accuracy using our weighted average metric with a threshold of 30°. When swimming in deep water mice lack a fixed, stable reference plane. While an animal with a subtle deficit might use feedback from the ground to maintain an upright posture when walking, this feedback is unavailable during swimming. Thus, natural swimming requires an increased reliance on vestibular feedback to maintain an upright position, making deficits more apparent. Indeed, it may be of interest in future studies to evaluate animal performance at different buoyancies, as this could further impact task difficulty.

The *Gpr156*$^{-/-}$ mutants chosen for this study exhibit impaired vestibular function, relying heavily on proprioceptive inputs, as shown by severe swimming defects despite normal performance on balance beam and other vestibular tests[19]. Specifically, we compared the performance of these *Gpr156*$^{-/-}$ mice with that of *Gpr156*$^{+/-}$ mice, since it has been established that the latter have normal protein expression and hair cell orientation[19]. Our finding that *Gpr156*$^{-/-}$ mutants demonstrate no deficits in balance beam testing compared to the *Gpr156*$^{+/-}$ mice suggests that their locomotion and inter-limb coordination during walking are well compensated for through the use of proprioceptive input. The selective swimming deficit observed in *Gpr156*$^{-/-}$ mice highlights the need for an objective, instrumented test to quantify performance during this task. Overall, quantitatively comparing swimming performance allows for objective assessment of behavioral deficits in mutant strains that can be compared across studies and laboratories. Finally, we note that the miniaturized IMU and headpost used in our study added negligible weight, a critical factor to ensure that task performance remains unaffected by the testing hardware itself.

In *Gpr156*$^{-/-}$ mutants, macular hair cells expressing the transcription factor EMX2 fail to undergo the usual reversal in hair cell orientation, disrupting the typical polarity and organization in otolith organs[18,27]. Although these EMX2-positive hair cells are normal in number, mechanotransduction ability, and afferent connectivity, they exhibit reversed directional sensitivity[19]. Consequently, the corresponding afferents likely show an opposite response to head movements compared to control animals. We speculate that the discrete functional deficit in *Gpr156*$^{-/-}$ mutants explains why they do not exhibit gross vestibular dysfunction, unlike mutants lacking normal vestibular hair bundles or associated mechanotransduction proteins. Deficits in other vestibular hair cell proteins, like GPR156, may contribute to vestibular function in specific ways that conventional tests like rotarod and balance beam can miss, since animals can utilize proprioceptive inputs. Compensatory changes in early vestibular pathways occur almost instantly following peripheral vestibular loss[28–30]. For instance, within 24 h of vestibular loss, neurons at the first stage of central processing in the vestibular nuclei upweight proprioceptive input. This proprioceptive sensory substitution aids compensation for impaired vestibular performance during active behaviors such as locomotion on a rotarod and balance beam[31,32]. However, due to reduced proprioceptive feedback, compensation during swimming is less complete. Thus, the ineffectiveness of proprioceptive substitution in aquatic environments underscores the importance of objective swim tests that objective and robustly quantify changes in behavioral performance.

Advancements from prior approaches

As discussed above, swim testing has been widely used to evaluate behavioral changes in a variety of studies spanning psychiatric research on depression and anxiety to functional deficits due to vestibular impairments. Traditionally, the evaluation of depression and anxiety in rodents using the Forced Swim Test (FST) has relied on manual scoring to measure immobility time, which is considered a key measure of behavioral despair.

Efforts to streamline analysis and enhance test precision have led to automated systems utilizing video analysis or photobeam arrays to detect and quantify behavior[33–42]. For example, Yuman et al.[38] proposed a high-speed video analysis method (240 fps) for FST to assess antidepressants and stress-evoked behavior. More recently, Nandi et al.[43] introduced a video-based method to automate FST analysis, and AI-based analysis approaches for tracking movement during open field tests combined with sophisticated video image processing (reviewed by Isik and Unal[44]) are increasingly popular and can be extended to quantify video during swimming[45]. These various video methods have a temporal resolution (< 30 fps) suitable for measuring immobility times, however may be unable to detect high-frequency movements during unstable swimming in mutant mice with vestibular impairments and are prone to image distortion at the air–water interface[46].

Our IMU-based approach offers precise and resource efficient tracking of motion with 6 degrees freedom (i.e., up/down, forward/back, left/right, pitch, roll, or yaw). This enables axis-specific analysis as well as dynamic spherical representation, thereby permitting precise evaluation of the multidimensional dynamics of complex swim behavior.

It is important to note that this method employs a 'zeroed' measurement taken while the animal is standing outside of water. Although our mutants showed no differences in baseline head movement relative to control mice[19], this point must be considered when testing mutant with significantly altered baseline head positions or resting tremors. Furthermore, we propose that, resource-permitting, that it would be valuable to employ the SWIMU method in combination with video measurement techniques to even more fully assess swimming behavior- measuring both visually apparent deficits (e.g. immobility, locomotive deficits) as well as multidimensional head movement deficits.

Directions for future work

An advantage of the SWIMU test is that it is relatively easy to implement, enabling non-specialist laboratories to obtain meaningful data readily. In contrast, vestibular sensory evoked potentials (VsEP), increasingly used to assess vestibular function in genetically modified mice, are less user-friendly and more challenging to

reproduce[47]. Like auditory brainstem responses (ABR) or visual evoked potentials (VEP), VsEPs are recorded with subcutaneous electrodes placed on the skull behind the mastoids. While VsEPs can directly and noninvasively evaluate early vestibular pathways, obtaining reliable recordings is challenging due to factors including the need for specialized equipment, expertise regarding electrode placement, and motion artifact removal[48].

Similar issues limit the quantification and evaluation of vestibular function via vestibulo-ocular reflex (VOR) eye movement testing[49]. The need for specialized equipment and expertise to properly perform VOR testing also hinders progress in the vestibular field, as reproducibility across laboratories is crucial. In this context, the SWIMU test is well-suited for screening genetically modified mice, especially with user-friendly software and analysis packages. We have detailed our device design in the "Methods" section and provided the MATLAB code for computing distributions, generating power spectra, and accessing dynamic orientation on GitHub (see "Methods"). Additionally, we note that in this study, we surgically implanted a head post on the skull of our mice to ensure the sensor was securely fastened during swimming, and thus accurately measuring the actual movement of the head relative to space. This placement, in turn, can be used to provide a representation of the activation of the vestibular sensory organs (semicircular canal and otoliths) during movement. Future studies using the SWIMU test could adopt less invasive approaches, such as attaching the miniature sensor using a custom-designed 3D-printed helmet and even body harness. A body harness combined with a head sensor moreover could also improve detection of and allow for quantitative description of head-on-neck movement difficulties in other animal models of non-vestibular dyscoordination, such as cerebellar deficits.

Beyond characterizing vestibular dysfunction, our quantitative SWIMU test could be valuable in other areas of neuroscience. For example, it could enhance the specificity of the forced swim test (FST), which assumes that an animal will initially attempt to escape when placed in water but will eventually show immobility, considered a measure of behavioral despair. Adapting our method would improve the FST's sensitivity by providing a more precise axis and frequency-specific readout of the animal's behavior throughout the test. Our method could similarly enhance the specificity of the Morris water maze[50], which tests spatial learning in rodents, by offering more detailed dynamic analyses of swimming patterns and spatial learning abilities. Additionally, the SWIMU method can enable comparative analysis of vestibular function across species. In zebrafish, for instance, the utricle is thought to be the primary vestibular organ[51,52,53] and proper vestibular function has been shown to be essential for the development of normal swimming behavior[54,53,55,56,57,58,59]. Coupled with our findings of swimming deficits in Gpr156 mutants with otolith-specific dysfunction, this suggests a potential ancestral role of the otolith organs in swimming function. By improving the quantification of swimming deficits in rodents, the SWIMU approach may facilitate cross-species comparisons to deepen our understanding of the vestibular basis of motion.

Lastly, our quantitative SWIMU approach could aid in protein discovery. Phenotyping facilities typically assess physiological and metabolic disorders in mice, including auditory brainstem response tests for hearing, but generally do not perform behavioral tests related to vestibular function. This gap, due to specialized equipment requirements and data reliability challenges, represents a missed opportunity for consortia like the Knockout Mouse Project (KOMP) and the International Mouse Phenotyping Consortium (IMPC), which generate and test numerous new mouse knockout strains. Implementing a quantitative swimming test could enhance phenotyping efforts, especially in drug screening and depression phenotyping, by providing comprehensive behavioral data linked to vestibular function.

Methods

Mice and genotyping

All animal experiments were carried out in accordance with the animal protocols approved by the Johns Hopkins University Animal Care and Use Committee (#MO20M172, #MO23M106) and ARRIVE guidelines. The *Gpr156*$^{-/-}$ mutant strain used in this study is the same constitutive inactivation used in[18,19]: *B6N(Cg)-Gpr156*$^{tm1.1(KOMP)Vlcg/J}$,MGI:5608696 produced by the Knockout Mouse Project consortium (KOMP). These mice are characterized by a lack of regional hair cell orientation reversal in otolith organs of the peripheral vestibular system. 10 *Gpr156* heterozygotes used as controls and 7 *Gpr156* homozygotes (mutants) mice were included in this study. The experimenter was blind to genotype during data collection as well as analysis for each of the tests detailed below.

Head-post surgery

A head post was implanted to ensure that the sensor was securely fastened to the animal's head during swimming. To implant the head post, mice were anesthetized with isoflurane (1–2%) and kept on a heating pad. Bupivacaine was used as a local anesthetic and injected under the scalp at the start of the surgery as well as at the end. An incision was made above the dorsal surface of the skull and the periosteum removed, and the stainless-steel post was chronically fastened above bregma on the skull using dental acrylic. Notably, this post was implanted such that the foreaft axis of the sensor aligned with the sagittal suture and the vertical axis laid perpendicular to the surface of the skull. Following the surgery, animals were isolated and carefully monitored for the first 48 hours.

Balance beam

The animal was given up to 2 min to cross 60 cm across a 6 mm wide beam to a dark box with food reward. If the animal falls off the beam, it is scored as a fail. 2 minutes were assigned for all animals that failed to traverse the 60 cm. 3 trials were done for each animal.

Contact inhibition of righting

The animal was placed in a small enclosed container such that all four of its feet are touching the bottom, and that its back is in contact with the upper surface. The container was then inverted so that the mouse was supine,

while the surface is still touching the soles of the animal's feet. The mouse's righting reflex was then graded based on the following scale:

- 0—animal rights successfully (no deficit);
- 1—partial righting, animal attempts to right (mild deficit);
- 2—complete loss of righting, animal walks with respect to the upper surface (severe deficit).

Every animal underwent 3 trials and the mode score was used for analysis.

Air righting

The animal was placed into a container at a height of 30–40 cm above a foam cushion. The container was quickly inverted such that the animal falls supine, and the air righting reflex was graded based on the following scale:

- 0—animal lands on its feet (no deficit);
- 1—animal lands on its side (mild deficit);
- 2—animal lands on its back (severe deficit).

Every animal underwent 3 trials and the mode score was used for analysis.

Tail hanging

The animal was held by the top of its tail and lowered close to an even surface. Its reflex was graded based on the following scale:

- 0—straight posture, extends forelimbs towards surface (no deficit);
- 1 – slight ventral bending of the body (mild deficit);
- 2—persistently bending the body or crawls up towards its tail (severe deficit).

Every animal underwent 3 trials and the mode score was used for analysis.

Rescue criteria for swim tests

In both scored and instrumented tests, animals freely swam for up to a minute or were rescued earlier if they met one of the following rescue criteria: (1) animal head was fully submerged for 3 consecutive seconds, or (2) animal stopped paddling and gave up (fatigue or stress response). Homozygote animals consistently required earlier rescue with an average of 17.4 ± 2.7 s to rescue, compared to 49.9 ± 3.0 s for the heterozygote controls[19].

Scored swim tests

The following criteria adapted from[15] were used to score swimming:

- 0—normal, body elongated and flagella-like tail motion (no deficit);
- 1—unbalanced swimming, loss of smooth movements (mild deficit);
- 2—underwater tumbling, unable to maintain upright position (severe deficit).

Each animal underwent 2–3 trials and the mode score was used for analysis.

Instrumented swim test

A miniature six-dimensional head motion sensor (TDK ICM-42688-P) comprising a three-dimensional (3D) accelerometer (measuring foreaft, lateral, and vertical axes accelerations) and a 3D gyroscope (measuring pitch, roll, and yaw angular velocity) was soldered to a small, custom circuit board, and coated in a thin layer of epoxy for waterproofing. Prior to recording, this was firmly affixed to a head-post implanted on the animal skull. Before being placed in the water, animals were held on a flat surface for 30 s for calibration. During the swim, animal head movement and orientation data was collected, as well as corresponding video data. Each animal underwent 2–3 trials.

The custom IMU circuit board was wired to an Arduino Teensy microcontroller (https://www.pjrc.com/store/) which read sensor data via an I2C bus from the IMU chip, and wrote it out via a USB serial port to a PC. Six-dimensional motion data was collected at 500 Hz using windows-based CoolTerm software. We then computed the power spectral densities (pwelch function, MATLAB, MathWorks) using Welch's averaged periodogram with nfft = 128 and a Bartlett window (128 ms duration) for all six dimensions of movement. Deviation from normality was quantified by the kurtosis (K) defined as:

$$K = \frac{\left\langle (X-\mu)^4 \right\rangle}{\sigma^4}$$

where μ and σ are the mean and standard deviation of the data X, respectively, and $<\cdots>$ is the average. The power between mutant and control mice was then compared over low and high frequency ranges, where the low frequency range was set from 0 to 5 Hz and the high frequency range was set from 5 to 20 Hz. The selection of 5 Hz was based on prior literature, which suggests during movement there exists separate power law relationships between frequency and power of movement after a transition frequency around 5-10 Hz. This suggests that vestibular signals encountered across daily activities are not scale invariant and this could play a role in the non-linearity of central vestibular neuron responses to natural stimuli[21]. In our results, we observed this transition

at 5 Hz. Moreover, the larger difference between mutants and control animals in the range of less than 5 Hz suggests that the difference between the two is larger scale animal movements that are slower in frequency and represent overall instability, versus higher frequency movements which may be more associated with muscle twitching or jerking.

To generate the spherical plots of the head orientation vector, MATLAB's imufilter facility was used. While differences in the raw inertial gyroscope and accelerometer signals were noted between mutant and normal populations, in general, the raw inertial signals can be difficult to work with. Linear accelerometers, for example, are sensitive to both linear accelerations, and also to gravity influences. The angular rate sensors (the "gyroscopes") give angular velocity, but do not keep track of overall orientation over time. To overcome these difficulties, a "sensor fusion" algorithm, such as Matlab's imufilter, uses a Kalman filter to fuse accelerometer and gyroscope data to estimate orientation of the IMU chip in space-fixed coordinates over time (see MATLAB documentation for imufilter). This will allow easier tracking of whether the mouse is keeping its head upright at all times.

Prior to processing, any inherent sensor signal offsets were subtracted out from the gyro signals while the IMU chip was not moving, and the signals were scaled to the units required by imufilter (accelerations were scaled to meters/sec^2, and angular velocity was scaled to radians/sec). Prior to the swim, the mouse remained still on a platform outside the tank, and the data during this time serves as the "zero" reference for the orientation estimates. This is to provide an initial value for the sensor-fusion algorithm. Moreover, the head post and IMU had negligible weight (0.17 g) relative to the weight of the animal. MATLAB's quat2rotm function was used to convert the quaternion output of imufilter into rotation matrices, which give directly the orthonormal X, Y, and Z vectors of the IMU's inertial frame. To compensate for the 45 degree upward pitched nose during swimming relative to their standing head position, the inertial frame was rotated by 45 degrees in the pitch plane, and the end point of the resulting Z "forehead" vector (which now points nominally upward relative to gravity while the mouse is swimming) was plotted three-dimensionally along with a wire-frame sphere (for easier visualization of the three-dimensional trace). Probability distribution functions were generated for each animal from this data of this vector's distance from upright across trials.

Using the probability distribution data shown in Fig. 6 Panel A, simple numerical classifier metric was derived, which separates the two mouse populations without error. The classifier metric is a simple weighted average of the Distance from Upright measure, weighted by the probability of each distance measure. It is computed by multiplying the X values (the "Distance from Upright") by the Y values (the probability for each deviation – ensuring that the Y values are "normalized" to sum to 1.0, as they should for a proper probability distribution), and summing together. Since this is a simple weighted average of deviations based on probability of occurrence, the units of this metric simply remain as "degrees" of deviation, and so can be plotted together on the same X axes with the probability traces. We show these computed metrics as a single dot for each swim trial, and color the dots the same as the corresponding probability trace, showing a clear separation between the normal (blue) and mutant (red) mice using a threshold of 30 degrees.

Statistics

Statistical significance was determined with a Wilcoxon rank sum test, or a permutation test for the power spectra analysis. Plotted are means +/- standard error of the mean unless otherwise stated, with the level of significance at $p < 0.05$. In figures, 'n.s.' stands for not significant.

Data availability

Sample data and MATLAB scripts to generate the sphere plots can be found at our GitHub repository (https://github.com/CullenLab/SWIMU_SwimTest/tree/main) along with instructions on how to run the scripts. The datasets analysed during the current study are available in this repository.

Received: 25 August 2024; Accepted: 18 November 2024
Published online: 26 November 2024

References

1. Stahl, J. S. Using eye movements to assess brain function in mice. *Vis. Res.* **44**(28), 3401–3410. https://doi.org/10.1016/j.visres.2004.09.011 (2004) (**PMID: 15536008**).
2. Ono, K. et al. Retinoic acid degradation shapes zonal development of vestibular organs and sensitivity to transient linear accelerations. *Nat. Commun.* **11**, 63. https://doi.org/10.1038/s41467-019-13710-4 (2020).
3. Luong, T. N., Carlisle, H. J., Southwell, A. & Patterson, P. H. Assessment of motor balance and coordination in mice using the balance beam. *J. Vis. Exp.* **49**, 2376. https://doi.org/10.3791/2376 (2011).
4. Lakes, E. H. & Allen, K. D. Gait analysis methods for rodent models of arthritic disorders: Reviews and recommendations. *Osteoarthr. Cartil.* **24**(11), 1837–1849. https://doi.org/10.1016/j.joca.2016.03.008 (2016).
5. Erway, L., Hurley, L. S. & Fraser, A. S. Congenital ataxia and otolith defects due to manganese deficiency in mice. *J. Nutr.* **100**(6), 643–654. https://doi.org/10.1093/jn/100.6.643 (1970).
6. Gray, L. E., Rogers, J. M., Ostby, J. S., Kavlock, R. J. & Ferrell, J. M. Prenatal dinocap exposure alters swimming behavior in mice due to complete otolith agenesis in the inner ear. *Toxicol. Appl. Pharmacol.* **92**, 266–273 (1988).
7. Sawada, I., Kitahara, M. & Yazawa, Y. Swimming test for evaluating vestibular function in guinea pigs. *Acta Otolaryngol. Suppl.* **510**, 20–23 (1994).
8. Sondag, H. N., De Jong, H. A., Van Marle, J. & Oosterveld, W. J. Behavioural changes in hamsters with otoconial malformations. *Acta Otolaryngol.* **118**, 86–89 (1998).
9. Akay, T., Tourtellotte, W. G., Arber, S. & Jessell, T. M. Loss of sensory feedback impairs locomotor pattern. *Proc. Natl. Acad. Sci.* **111**(47), 16877–16882. https://doi.org/10.1073/pnas.1419045111 (2014).
10. Gruner, J. A. & Altman, J. Swimming in the rat: Analysis of locomotor performance in comparison to stepping. *Exp. Brain Res.* **40**(4), 374–382. https://doi.org/10.1007/BF00236146 (1980) (**PMID: 7439281**).

11. Vidal, P. P., Degallaix, L., Josset, P., Gasc, J. P. & Cullen, K. E. Postural and locomotor control in normal and vestibularly deficient mice. *J. Physiol.* **559**(Pt 2), 625–638. https://doi.org/10.1113/jphysiol.2004.063883 (2004).
12. Manes, M. et al. Behavioral and neurochemical characterization of the mlh mutant mice lacking otoconia. *Behav. Brain Res.* **1**(359), 958–966. https://doi.org/10.1016/j.bbr.2018.06.012 (2019) (**Epub 2018 Jun 18 PMID: 29913187**).
13. Kaiser, A. et al. Auditory and vestibular defects in the circling (*ci2*) rat mutant. *Eur. J. Neurosci.* **14**, 1129–1142. https://doi.org/10.1046/j.0953-816x.2001.01726.x (2001).
14. Rabbath, G. et al. Abnormal vestibular control of gaze and posture in a strain of a waltzing rat. *Exp. Brain Res.* **136**(2), 211–223. https://doi.org/10.1007/s002210000568 (2001).
15. Hardisty-Hughes, R., Parker, A. & Brown, S. A hearing and vestibular phenotyping pipeline to identify mouse mutants with hearing impairment. *Nat. Protoc.* **5**, 177–190. https://doi.org/10.1038/nprot.2009.204 (2010).
16. Wu, X. et al. Allicin protects against cisplatin-induced vestibular dysfunction by inhibiting the apoptotic pathway. *Eur. J. Pharmacol.* **15**(805), 108–117. https://doi.org/10.1016/j.ejphar.2017.02.052 (2017) (**PMID: 28259711**).
17. Minasyan, A. et al. Vestibular dysfunction in vitamin D receptor mutant mice. *J. Steroid Biochem. Mol. Biol.* **114**(3–5), 161–166. https://doi.org/10.1016/j.jsbmb.2009.01.020 (2009) (**PMID: 19429446**).
18. Kindt, K. S. et al. EMX2-GPR156-Gαi reverses hair cell orientation in mechanosensory epithelia. *Nat. Commun.* **12**(1), 2861. https://doi.org/10.1038/s41467-021-22997-1 (2021).
19. Ono, K. et al. Contributions of mirror-image hair cell orientation to mouse otolith organ and zebrafish neuromast function. *eLife* https://doi.org/10.7554/eLife.97674.1 (2024).
20. Zobeiri, O. A., Ostrander, B., Roat, J., Agrawal, Y. & Cullen, K. E. Loss of peripheral vestibular input alters the statistics of head movement experienced during natural self-motion. *J. Physiol.* **599**, 2239–2254. https://doi.org/10.1113/JP281183 (2021).
21. Carriot, J., Jamali, M., Chacron, M. J. & Cullen, K. E. The statistics of the vestibular input experienced during natural self-motion differ between rodents and primates. *J. Physiol.* **595**(8), 2751–2766. https://doi.org/10.1113/JP273734 (2017).
22. Can, A. et al. The mouse forced swim test. *J. Vis. Exp* **59**, e3638. https://doi.org/10.3791/3638 (2012).
23. Ji, Y. R. et al. Function of bidirectional sensitivity in the otolith organs established by transcription factor Emx2. *Nat. Commun.* **13**(1), 6330. https://doi.org/10.1038/s41467-022-33819-3 (2022).
24. Li, Y., Liu, S., Teng, Q., Gong, S. & Liu, K. A method for constructing a mouse model of congenital hearing loss by bilateral cochlear ablation. *J. Neurosci. Methods.* **378**, 109641. https://doi.org/10.1016/j.jneumeth.2022.109641 (2022).
25. Jiang, W. et al. Notch signaling pathway plays a critical role in chemotherapeutic drug-induced vestibular injury. *Biosci. Trends.* **16**(5), 363–366. https://doi.org/10.5582/bst.2022.01394 (2022).
26. Vartanian, V. et al. Spontaneous allelic variant in deafness-blindness gene Ush1g resulting in an expanded phenotype. *Genes Brain Behav.* **22**(4), e12849. https://doi.org/10.1111/gbb.12849 (2023).
27. Jiang, T., Kindt, K. & Wu, D. K. Transcription factor Emx2 controls stereociliary bundle orientation of sensory hair cells. Nathans J, ed.. *eLife.* **6**, e23661. https://doi.org/10.7554/eLife.23661 (2017).
28. Sadeghi, S. G., Minor, L. B. & Cullen, K. E. Neural correlates of motor learning in the vestibulo-ocular reflex: Dynamic regulation of multimodal integration in the macaque vestibular system. *J. Neurosci.* **30**(30), 10158–10168. https://doi.org/10.1523/JNEUROSCI.1368-10.2010 (2010).
29. Sadeghi, S. G., Minor, L. B. & Cullen, K. E. Neural correlates of sensory substitution in vestibular pathways following complete vestibular loss. *J. Neurosci.* **32**(42), 14685–14695. https://doi.org/10.1523/JNEUROSCI.2493-12.2012 (2012).
30. Sadeghi, S. G., Minor, L. B. & Cullen, K. E. Multimodal integration after unilateral labyrinthine lesion: Single vestibular nuclei neuron responses and implications for postural compensation. *J. Neurophysiol.* **105**(2), 661–673 (2011).
31. Jamali, M. et al. Neuronal detection thresholds during vestibular compensation: Contributions of response variability and sensory substitution. *J. Physiol.* **592**(7), 1565–1580. https://doi.org/10.1113/jphysiol.2013.267534 (2014).
32. Carriot, J., Jamali, M. & Cullen, K. E. Rapid adaptation of multisensory integration in vestibular pathways. *Front. Syst. Neurosci.* **9**, 59. https://doi.org/10.3389/fnsys.2015.00059 (2015).
33. Hédou, G., Pryce, C., Di Iorio, L., Heidbreder, C. A. & Feldon, J. An automated analysis of rat behavior in the forced swim test. *Pharmacol. Biochem. Behav.* **70**(1), 65–76. https://doi.org/10.1016/S0091-3057(01)00575-5 (2001).
34. Kurtuncu, M., Luka, L. J., Dimitrijevic, N., Uz, T. & Manev, H. Reliability assessment of an automated forced swim test device using two mouse strains. *J. Neurosci. Methods.* **149**(1), 26–30. https://doi.org/10.1016/j.jneumeth.2005.04.010 (2005).
35. Rocha, B. A., Fleischer, R., Schaeffer, J. M., Rohrer, S. P. & Hickey, G. J. 17β-estradiol-induced antidepressant-like effect in the forced swim test is absent in estrogen receptor-β knockout (BERKO) mice. *Psychopharmacology.* **179**(3), 637–643. https://doi.org/10.1007/s00213-004-2078-1 (2005).
36. Cryns, K. et al. Lack of lithium-like behavioral and molecular effects in IMPA2 knockout mice. *Neuropsychopharmacol.* **32**(4), 881–891. https://doi.org/10.1038/sj.npp.1301154 (2007).
37. Juszczak, G. R., Lisowski, P., Śliwa, A. T. & Swiergiel, A. H. Computer assisted video analysis of swimming performance in a forced swim test: Simultaneous assessment of duration of immobility and swimming style in mice selected for high and low swim-stress induced analgesia. *Physiol. Behav.* **95**(3), 400–407. https://doi.org/10.1016/j.physbeh.2008.07.003 (2008).
38. Yuman N, Idaku I, Kenkichi Y, Takeshi T, Kensuke O, Hiroshi M. High-speed video analysis of laboratory rats behaviors in forced swim test. In: *2008 IEEE International Conference on Automation Science and Engineering*. 206–211. https://doi.org/10.1109/COASE.2008.4626501 (2008)
39. Kulikov, A., Morozova, M., Kulikov, V., Kirichuk, V. & Popova, N. Automated analysis of antidepressants' effect in the forced swim test. *J. Neurosci. Methods* **191**, 26–31. https://doi.org/10.1016/j.jneumeth.2010.06.002 (2010).
40. Hayashi, E., Shimamura, M., Kuratani, K., Kinoshita, M. & Hara, H. Automated experimental system capturing three behavioral components during murine forced swim test. *Life Sci.* **88**(9), 411–417. https://doi.org/10.1016/j.lfs.2010.12.016 (2011).
41. Gao, V., Vitaterna, M. H. & Turek, F. W. Validation of video motion-detection scoring of forced swim test in mice. *J. Neurosci. Methods* **235**, 59–64. https://doi.org/10.1016/j.jneumeth.2014.06.002 (2014).
42. Sturman, O. et al. Deep learning-based behavioral analysis reaches human accuracy and is capable of outperforming commercial solutions. *Neuropsychopharmacology* **45**(11), 1942–1952. https://doi.org/10.1038/s41386-020-0776-y (2020).
43. Nandi, A., Virmani, G., Barve, A. & Marathe, S. DBscorer: An open-source software for automated accurate analysis of rodent behavior in forced swim test and tail suspension test. *eNeuro* https://doi.org/10.1523/ENEURO.0305-21.2021 (2021).
44. Isik, S. & Unal, G. Open-source software for automated rodent behavioral analysis. *Front. Neurosci.* **17**, 1149027. https://doi.org/10.3389/fnins.2023.1149027 (2023).
45. Khunarsar P, Benjathum N, Charoenpong T, Jarivapongskul A. A method of swimming rat detection in morris water maze by using image processing, 2018 International Electrical Engineering Congress (iEECON), pp. 1–4, 2018.
46. Shortis, M. Camera calibration techniques for accurate measurement underwater. In *3D Recording and Interpretation for Maritime Archaeology* (eds McCarthy, J. K. et al.) (Springer, Berlin, 2019). https://doi.org/10.1007/978-3-030-03635-5_2.
47. Jones, T. A. et al. The adequate stimulus for mammalian linear vestibular evoked potentials (VsEPs). *Hear Res.* https://doi.org/10.1016/j.heares.2011.05.005 (2011).
48. Honaker, J. A., Lee, C., Criter, R. E. & Jones, T. A. Test-retest reliability of the vestibular sensory-evoked potential (VsEP) in C57BL/6J mice. *J. Am. Acad. Audiol.* **26**(1), 59–67. https://doi.org/10.3766/jaaa.26.1.7 (2015).
49. Stahl, J. S., van Alphen, A. M. & De Zeeuw, C. I. A comparison of video and magnetic search coil recordings of mouse eye movements. *J. Neurosci. Methods.* **99**(1–2), 101–110. https://doi.org/10.1016/s0165-0270(00)00218-1.PMID (2000).

50. Vorhees, C. & Williams, M. Morris water maze: Procedures for assessing spatial and related forms of learning and memory. *Nat. Protoc.* **1**, 848–858. https://doi.org/10.1038/nprot.2006.116 (2006).
51. Baeza-Loya, S. & Raible, D. W. Vestibular physiology and function in zebrafish. *Front Cell Dev. Biol.* https://doi.org/10.3389/fcell.2023.1172933 (2023).
52. Riley, B. B. & Moorman, S. J. Development of utricular otoliths, but not saccular otoliths, is necessary for vestibular function and survival in zebrafish. *J. Neurobiol.* **43**(4), 329–337. https://doi.org/10.1002/1097-4695(20000615)43:4%3c329::aid-neu2%3e3.0.co;2-h (2000).
53. Bagnall, M. W. & Schoppik, D. Development of vestibular behaviors in zebrafish. *Curr. Opin. Neurobiol.* **53**, 83–89. https://doi.org/10.1016/j.conb.2018.06.004 (2018).
54. Ehrlich, D. E. & Schoppik, D. A primal role for the vestibular sense in the development of coordinated locomotion. *Elife.* **8**, e45839. https://doi.org/10.7554/eLife.45839 (2019).
55. Hamling, K. R., Harmon, K., Kimura, Y., Higashijima, S. & Schoppik, D. The vestibulospinal nucleus is a locus of balance development. *J. Neurosci.* https://doi.org/10.1523/JNEUROSCI.2315-23.2024 (2024).
56. Bagnall, M. W. & McLean, D. L. Modular organization of axial microcircuits in zebrafish. *Science (New York, NY).* **343**(6167), 197. https://doi.org/10.1126/science.1245629 (2014).
57. Liu, Z. et al. Organization of the gravity-sensing system in zebrafish. *Nat. Commun.* **13**, 5060. https://doi.org/10.1038/s41467-022-32824-w (2022).
58. Beiza-Canelo, N. et al. Magnetic actuation of otoliths allows behavioral and brain-wide neuronal exploration of vestibulo-motor processing in larval zebrafish. *Curr. Biol.* **33**(12), 2438-2448.e6. https://doi.org/10.1016/j.cub.2023.05.026 (2023).
59. Favre-Bulle, I. A., Stilgoe, A. B., Rubinsztein-Dunlop, H. & Scott, E. K. Optical trapping of otoliths drives vestibular behaviours in larval zebrafish. *Nat. Commun.* **8**(1), 630. https://doi.org/10.1038/s41467-017-00713-2 (2017).
60. Sugioka, T., Tanimoto, M. & Higashijima, S. I. Biomechanics and neural circuits for vestibular-induced fine postural control in larval zebrafish. *Nat. Commun.* **14**(1), 1217. https://doi.org/10.1038/s41467-023-36682-y (2023).
61. Sadeghi, S. G. & Géléoc, G. S. G. Editorial: Commonalities and differences in vestibular and auditory pathways. *Front. Neurosci.* **16**, 876798. https://doi.org/10.3389/fnins.2022.876798 (2022).

Author contributions

NCH performed acquisition, analysis, and interpretation of data including new code development and wrote manuscript text and assisted in subsequent substantive revisions. DCR aided in acquisition, analysis, and interpretation of data including new code development. BT similarly assisted in acquisition and interpretation of data including provision of mice as well as substantial revisions of work. KEC was responsible for conception and design, oversight of acquisition, analysis, and interpretation of data, and writing manuscript text and substantive revisions.

Declarations

Competing interests

The authors declare no competing interests.

Additional information

Correspondence and requests for materials should be addressed to K.E.C.

Reprints and permissions information is available at www.nature.com/reprints.

Publisher's note Springer Nature remains neutral with regard to jurisdictional claims in published maps and institutional affiliations.